Meridional Overturning Circulation transport variability at 34.5°S during 2009-2017: Baroclinic and barotropic flows and the dueling influence of the boundaries

Christopher S. Meinen[1], Sabrina Speich[2], Alberto R. Piola[3,4,5], Isabelle Ansorge[6], Edmo Campos[7,8], Marion Kersalé[9,1], Thierry Terre[10], Maria Paz Chidichimo[3,5], Tarron Lamont[11,6], Olga T. Sato[7], Renellys C. Perez[1], Daniel Valla[3,5], Marcel van den Berg[11], Matthieu Le Hénaff[9,1], Shenfu Dong[1], and Silvia L. Garzoli[9,1]

[1]Atlantic Oceanographic and Meteorological Laboratory, Miami, USA
[2]Laboratoire de Météorologie Dynamique – IPSL, Ecole Normale Supérieure, Paris, France
[3]Servicio de Hidrografía Naval, Buenos Aires, Argentina
[4]Universidad de Buenos Aires, Buenos Aires, Argentina
[5]Instituto Franco-Argentino sobre Estudios de Clima y sus Impactos, Consejo Nacional de Investigaciones Científicas y Técnicas (CONICET), Argentina
[6]Oceanography Department and the Marine Research Institute (MA-RE), University of Cape Town, Rondebosch 7701, South Africa
[7]Oceanographic Institute, University of São Paulo, São Paulo, Brazil
[8]Ocean Sciences Laboratory, Federal University of Ceará, Brazil
[9]Cooperative Institute for Marine and Atmospheric Studies, University of Miami, Miami, USA
[10]IFREMER, Univ. Brest, CNRS, IRD, Laboratoire d'Océanographie Physique et Spatiale (LOPS), IUEM, Plouzané, France
[11]Oceans and Coasts Research Branch, Department of Environmental Affairs, Cape Town, South Africa

Key Points:

- The meridional overturning circulation at 34.5°S has significant variability at time scales ranging from daily to interannual.
- Seasonal variations of the meridional overturning circulation at 34.5°S are driven primarily by density variations at the eastern boundary.
- Interannual variations of the meridional overturning circulation at 34.5°S have significant baroclinic and barotropic contributions.

This article has been accepted for publication and undergone full peer review but has not been through the copyediting, typesetting, pagination and proofreading process which may lead to differences between this version and the Version of Record. Please cite this article as doi: 10.1029/2018GL077408

Abstract:

Six years of simultaneous moored observations near the western and eastern boundaries of the South Atlantic are combined with satellite winds to produce a daily time series of the basin-wide meridional overturning circulation (MOC) volume transport at 34.5°S. The results demonstrate that barotropic and baroclinic signals at both boundaries cause significant transport variations, and as such must be concurrently observed. The data, spanning ~20 months during 2009-2010 and ~4 years during 2013-2017, reveal a highly energetic MOC record with a temporal standard deviation of 8.3 Sv, and strong variations at time scales ranging from a few days to years (peak-to-peak range = 54.6 Sv). Seasonal transport variations are found to have both semi-annual (baroclinic) and annual (Ekman and barotropic) timescales. Interannual MOC variations result from both barotropic and baroclinic changes, with density profile changes at the eastern boundary having the largest impact on the year-to-year variations.

Introduction:

Variability in the meridional overturning circulation (MOC) is correlated with important worldwide climate variations, including changes in precipitation patterns, air temperatures, coastal sea levels, and extreme weather events (e.g. Vellinga and Wood, 2002; Stouffer et al., 2006; Latif et al., 2007; McCarthy et al., 2015a; Lopez et al., 2016). Theoretical and observational studies of the mechanisms controlling the MOC in the Atlantic have suggested that the MOC is presently bistable, with on and off states, and that MOC stability is controlled by interocean exchange between the South Atlantic and Southern Oceans (e.g. Dijkstra, 2007; Huismann et al., 2010; Drijfhout et al., 2011; Garzoli et al., 2013). While continuous, daily, observations of the MOC have been ongoing for 13+ years in the North Atlantic at 26.5°N (e.g. Kanzow et al., 2007; McCarthy et al., 2015b; Frajka-Williams et al.,

2016; Smeed et al., 2018), observations of the MOC in the South Atlantic have been limited mainly to repeated quasi-synoptic snapshot ship sections using either expendable bathythermograph (XBT) probes (e.g. Garzoli and Baringer, 2007; Dong et al., 2009) or full-depth conductivity-temperature-depth (CTD) profiles (e.g. Lumpkin and Speer, 2007; Bryden et al., 2011; McCarthy et al., 2011), and to indirect estimates combining satellite observations with irregularly spaced (in time and space) hydrographic data (e.g. Dong et al., 2015; Majumder et al., 2016). While these studies have greatly improved our understanding of the MOC structure and dynamics (e.g. Garzoli and Matano, 2011; Buckley and Marshall, 2016), the daily MOC observations at 26.5°N have illustrated the importance of continuous observations to avoid aliasing highly energetic short period variations (e.g., Kanzow et al., 2010).

A preliminary effort at estimating the daily variations in the MOC at 34.5°S was published by Meinen et al. (2013; hereafter MEA13) involving the first 20-months of data and, by necessity, focusing on sub-annual time scale variability. The western boundary study described in that paper has continued to date, focusing on western boundary current transport variations (e.g. Meinen et al., 2012; 2017). The eastern boundary study ended in December 2010, but was restarted in September 2013 with significant enhancements and new partners (e.g. Ansorge et al., 2014; Kersalé et al., 2018). With the restart of the eastern array, it is now possible to update the daily MOC record with an additional ~4 years of continuous data (September 2013-April 2017) following MEA13 and studying seasonal to interannual MOC variations at 34.5°S. The purpose of this article is to highlight several key results of this new analysis, and to contrast the results with previously published results from 26.5°N.

Data and Methods:

The standard method for estimating the MOC from moored instrumentation is to capture a continuous time series of density profiles on either side of the basin along a line of latitude and to use thermal wind to estimate the profile of meridional flow across that line relative to an assumed level of no motion (e.g. Kanzow et al., 2007; McCarthy et al., 2015b). To this geostrophic integral, the boundary flows and an estimate of the Ekman transport are added. The final component, the 'barotropic contribution', has traditionally been determined as a residual based on the assumption of zero-net-flow when the meridional velocity is integrated across the basin and from surface to seafloor (e.g. McCarthy et al., 2015b). MEA13 approached this 'barotropic' term differently, using measured bottom pressure on either side of the basin to directly estimate absolute geostrophic velocity fluctuations (but not the time-mean) that could be added to the relative geostrophic velocity profiles. Furthermore, rather than obtaining the density profiles on either side of the basin via 'dynamic height moorings' (e.g. Rayner et al., 2011), the MEA13 study utilized pressure-equipped inverted echo sounder (PIES) moorings at roughly the 1350 dbar isobath to estimate full-water-column profiles of temperature, salinity, and density on either side of the basin via the Gravest Empirical Mode method (Meinen and Watts, 2000). A previous model-based analysis demonstrated that this approach would be effective at capturing the MOC volume transport at 34.5°S (Perez et al., 2011).

For the present study, data from PIES near the western and eastern boundaries (Figure 1a) are used (following the MEA13 methodology) to estimate both the geostrophic relative ("baroclinic") and geostrophic reference ("barotropic") components of the meridional transports between Sites A and Z. The Ekman component of the meridional transport between A and Z is estimated using the cross-calibrated multi-platform (CCMP) wind product version

2.0 (Atlas et al., 1996, 2011; Hoffman et al., 2013; Wentz et al., 2015). To account for the total (geostrophic plus Ekman) meridional transport inshore of A and Z, the time-mean flow from the output of a 35-year run of the Ocean For the Earth Simulator (OFES) numerical model (Masumoto et al., 2004, Sasaki et al., 2008) is used. This OFES product, available as 3-day snapshots, is a longer-run, provided at a higher horizontal resolution (0.1° versus 0.2°), than was available for the earlier MEA13 study. The same longer OFES output is used to estimate the time-mean reference velocity flow integrated between the 1350 dbar isobaths across the basin interior; recall that the observed bottom pressure differences give the reference velocity time variability only. The increased model resolution and run length has little impact on the time-mean reference velocity integrated between the 1350 dbar isobaths; it also does not significantly affect the temporal standard deviations (σ) of the model flows inshore of A and Z (utilized for the error analysis only). It does, however, significantly alter the time-mean flow estimates inshore of Sites A and Z. The data from the original MEA13 study has been reanalyzed here using these new inshore mean flow estimates. Finally, the boundary, baroclinic, barotropic, and Ekman terms are combined and integrated down to the time-varying pressure interface where the zonally-integrated meridional flow changes from northward to southward (interface time-mean = 1160 dbar; σ = 175 dbar) to get the total MOC transport.

Results and Discussion:

As mentioned earlier, the acoustic travel time and bottom pressure measurements made by PIES moorings can be considered measures of the baroclinic and barotropic ocean variability, respectively. Visual comparisons of both the travel time (Figure 1b) and the bottom pressure (Figure 1c) records suggest that the ocean is more energetic in the west (Site A) than it is in the east (Site Z). Spectral analysis of the travel time records confirms that this is true at all

time scales from periods of a few days to two years (Figure 1d). This stronger travel time variability at A is likely due to the variability of the separation of the Brazil Current from the coast (e.g. Olson et al., 1988; Goni et al., 2011). Interestingly, for the bottom pressure (Figure 1e), the western record is clearly more energetic at most time scales, but the eastern record is more energetic at periods longer than about 200 days. Site Z is well inshore of the Agulhas Ring corridor (e.g. Garzoli and Gordon, 1996), so the strong barotropic variations between 120 and 730 days are most likely not associated with passage of those rings, but could be associated with pulses from the Agulhas retroflection, or with eddies forming along the upwelling front coincident with the continental slope (Hall and Lutjeharms, 2011). The stronger pressure (barotropic) variations at A at periods less than 200 days likely reflect both the influence of the Brazil Current and the Deep Western Boundary Current just offshore (e.g. Meinen et al. 2012, 2017). At annual and semi-annual periods, there is little energy in either the travel time (baroclinic) or bottom pressure (barotropic) record at A (Figures 1d,e). By contrast, the bottom pressure record at Z has a broad, strong, peak in the spectra centered at the annual period.

The MOC volume transport time series, calculated here following the methods of MEA13, has a peak-to-peak range of 54.6 Sv from a maximum northward transport of 43.4 Sv to a minimum southward transport of -11.2 Sv (Figure 2). The mean meridional transport over the full 2009-2017 period (keeping in mind the ~3 year gap during Dec. 2010-Sep. 2013) is 14.7 Sv. As noted earlier, the time-mean MOC estimate following the MEA13 methods is highly dependent on the time-mean inshore flows and the time-mean reference velocity from OFES, and is therefore the least reliable part of the calculation. By contrast, the MOC transport anomalies are far more robust, being wholly based on observations. As such MOC transport anomalies are the focus of this study.

Contributions to the variability

There are strong MOC variations at time scales of a few days to a few weeks (Figure 2), highlighting the strength of a temporally continuous observing system. The daily MOC σ at 34.5°S, 8.3 Sv, exceeds the MOC σ at 26.5°N (σ ~ 5 Sv; e.g. Cunningham et al., 2007; McCarthy et al., 2015b). This higher variability is partially due to the fact that the 26.5°N array estimate has an inherent 10-day low-pass filter applied to it as part of the processing (e.g. Kanzow et al., 2007). Applying a similar 10-day low-pass filtering to the 34.5°S time series (2nd order Butterworth, passed both forward and back) yields a significantly reduced σ (7.0 Sv). Following MEA13, the daily MOC estimates in this study are accurate to within a random error of 5.9 Sv.

There is little difference between the MOC σ calculated over the first 20 months (8.9 Sv; MEA13) and the value calculated over the full record, 8.3 Sv, highlighting the dominant role of the high-frequency variations. This variability is most strongly driven by the geostrophic relative velocity contribution to the MOC (Figure 2; σ = 6.0 Sv), with the Ekman contribution (σ = 4.7 Sv) and the geostrophic reference velocity contribution (σ = 4.6 Sv) playing roughly equivalent secondary roles. The dominance of the relative variations is also borne out by comparison of the correlation between the total MOC and the relative velocity contribution (r = 0.71), as compared with the Ekman (r = 0.51) and reference velocity (r = 0.35) contributions. Since these MOC components are uncorrelated with one another (correlations r ≤ 0.20), the results illustrate the need for observing all three terms.

Breaking down the relative and reference terms into the contributions from the western and eastern boundary density and pressure variations illustrates significant differences between the MOC as observed at 34.5°S and at 26.5°N. At 26.5°N the relative component of the

MOC is dominated by density variations at the western boundary at all time scales other than seasonal (e.g. Chidichimo et al., 2010; McCarthy et al., 2015b). At 34.5°S, the relative component is roughly equally controlled by density variations on the western side (Figure 2; σ = 4.1 Sv) and on the eastern side (σ = 4.6 Sv). This important role of density variations at both boundaries reflects the impact of interocean exchanges between South Atlantic and Indian waters (e.g. de Ruijter et al., 1999) and/or Pacific waters (e.g. Rintoul, 1991; Sloyan and Rintoul, 2001). The reference term is also roughly equally controlled by variations on the western and eastern sides (σ = 7.9 Sv and 8.7 Sv, respectively). The higher variability of the pressure contributions (when holding one side constant) compared to the density contributions likely results from the energetic short period nature of barotropic signals. Much of this increased pressure variability occurs concurrently across the basin, evident from the high correlation between the daily western and eastern pressure contributions (r = 0.76). The relative (density) terms also experience correlated variations between A and Z (r = 0.63), albeit weaker.

Seasonal variations

The earlier MEA13 study had too short of a record (20 months) to study the seasonal cycle of the MOC. With four additional years of daily data, it is now possible to evaluate the MOC seasonal cycle at 34.5°S (Figure 3a). The resulting total MOC seasonal cycle has something of a semi-annual period to it, with maxima in northward transport in early austral summer (December-January) and for an extended period centered on austral winter (May-September), and minima in austral fall (February-March) and spring (October-November). This semi-annual period has not been observed by prior studies of the MOC variability at this latitude using XBT transect data (e.g. Dong et al., 2009; Garzoli et al., 2013), Argo/hydrography climatology (Dong et al., 2014) or Argo-altimetry merged data (e.g. Dong et al., 2015;

Majumder et al., 2016), all of which found more of an annual period to the seasonal MOC variations, although it should be noted that the phasing of those previously derived annual cycles are not all in agreement. It is possible that the semi-annual seasonal cycle determined from the PIES moorings here is due to 'statistical noise' given that only ~6 years of data are available. The variance of the 2013-2017 continuous MOC record high-pass filtered for short periods (< 70 days) exceeds the variance of the band passed MOC variability centered around the semi-annual (170-190 days) and annual (355-375 days) periods by more than a factor of three (not shown), highlighting the challenge of extracting a seasonal cycle from the 'noisy' record. Note these energetic high-frequency signals have likely also aliased previous observational results based on temporally irregular data. Numerical modeling results in the Agulhas Current have suggested a significant semi-annual period in that flow (e.g. Hermes et al., 2007), which feeds some of the warm upper limb MOC flow, so a semi-annual MOC signal at 34.5°S is not unexpected.

Assuming that the seasonal signal resolved from the 6 years of daily PIES data is robust, the difference between the mooring-based MOC seasonal cycle and previous estimates must be due to differences in one (or more) of the constituent time series. The Ekman transport seasonality (Figure 3a) is annual and is fairly consistent in both amplitude and phase with that observed previously using other wind products (e.g. Dong et al., 2014; 2015). Of the two geostrophic components (relative and reference), the geostrophic relative velocity term clearly has a semi-annual component to it, and agrees in phase and amplitude with the total MOC variability. The geostrophic relative MOC seasonal cycle found here is different from what has been termed the 'geostrophic' variability in previous studies in both time scale (semi-annual versus annual) and phasing.

One reason for the difference between this study and previous studies may lie in how those earlier studies calculated their 'geostrophic' term. In the cases of the XBT, Argo-climatology, and Argo-altimetry studies cited above, the 'geostrophic' term was calculated by subtracting the Ekman flow from the 'fully-adjusted' MOC estimate. 'Fully-adjusted' in this context indicates that the MOC in those studies has been calculated utilizing a residual method to estimate the barotropic component of the flow. Those studies therefore include their 'residual barotropic' term inextricably intertwined with their geostrophic thermal-wind-based density gradient term (herein called 'relative'). As is the nature of residual calculations, the 'geostrophic' term in those previous studies also accumulates any errors in the Ekman and boundary transports, and any errors resulting from data coverage limitations (e.g. below 850 m for the XBT data). As such, it is difficult to diagnose the reason for the disparity between annual seasonality in the prior studies versus semi-annual in the relative term estimated here. Hopefully, longer records and analyses using numerical models will aid in diagnosing this apparent contradiction.

Because the present study does not use a residual method, and obtains the reference (barotropic) velocity variability directly from data (bottom pressure gradients), it is possible for the first time to directly estimate the seasonal cycle of this term from data. The seasonal cycle of the reference term (Figure 3a) is fairly annual, with 3 months of southward anomalies in austral winter, and it is roughly 180° out of phase with the annual seasonal cycle in the Ekman term. This near compensation between the Ekman and reference terms is exciting because the two terms result from completely independent data sets. It also illustrates why the total MOC seasonal cycle is primarily controlled by the trans-basin density gradients.

The relative and reference seasonal cycles can be broken up to evaluate the contribution of the west and east density and pressure variations (Figure 3b). Despite the travel time spectra (Figure 1d) suggesting that there was significantly more energy in the west at all periods, the seasonal variability of the relative MOC term is clearly controlled by semi-annual density variations near the eastern boundary (Figure 3b). The strong annual signal in the reference component seasonal cycle (Figure 3a) is clearly dominated by the pressure at the eastern boundary (Figure 3b), although the significant mixed annual/semi-annual pressure signal at the western boundary (Figure 3b) clearly modulates and changes the phasing of the reference seasonal cycle.

Interannual variations

Interannual signals in the MOC can be difficult to observe in the daily time series due to the large variance associated with shorter time scales – the variance of the high pass filtered MOC time series with a cutoff period of 170 days (71.6 Sv^2) is nearly an order of magnitude larger than the variance of the low pass filtered MOC time series with a cutoff period of 375 days (8.4 Sv^2). These interannual variations become much more apparent when looking at the calendar-year annual averages (Table 1). The MOC annual averages exhibit a fairly wide range, from 4.6 Sv ± 1.7 Sv (mean ± standard error, hereafter SEM, see Table 1) of anomalous northward transport to -3.8 Sv ± 1.7 Sv of anomalous southward transport. (Note: the 4.6 Sv anomaly in 2009 is based on only ~9.5 months of data; correcting for the missing portion of the seasonal cycle would reduce this value by roughly 0.6 Sv.) Breaking out the annual mean anomalies of the various contributions to the MOC yields several important facts. Large annual anomalies (exceeding the SEM) are just as often dominated by the relative (density) term as by the reference (pressure) term, although the two largest amplitude anomalies are both caused by the relative term. Focusing on years with at least nine months

of data, the relative term dominates the MOC variability for the large positive and negative anomalies in 2009 and 2014, while the negative anomaly in 2010 and the positive anomaly in 2015 are primarily driven by the reference term. This again highlights the essential nature of observing both components. Neglecting 2013 and 2017, when only three and four months of data are available, respectively, the Ekman annual anomalies are quite small.

Breaking out the relative and reference terms once again into the contributions from the western and eastern density and pressure (Table 1), it becomes evident that in years when the relative term is small compared to the reference term it is because the eastern and western density terms are of opposite sign and nearly cancel (e.g., 2010, 2015, 2016). In the years when the relative term dominates over the reference term (e.g., 2009, 2014), the eastern density contribution is ~50% larger than the western density contribution, but both are large enough to be important and they are of the same sign. This is despite the fact that the western boundary travel time variability greatly exceeds that of the eastern boundary at time scales beyond annual (Figure 1d). Thus, for interannual variability, it is often the density variations on the eastern boundary that are most crucial for the MOC, which contrasts the results at 26.5°N where the western boundary density variations tend to dominate at that time scale (e.g. McCarthy et al., 2015b). For the years when the reference contribution dominates, by contrast, the contributions of the western and eastern pressure variability are of the same sign but can differ in magnitude by a factor of 3-4 (2010) or be roughly equal (2015).

Conclusions:

By contrast with 26.5°N, where the non-Ekman components of MOC variability appear to be primarily driven by western boundary changes at all time scales aside from seasonal (e.g. Chidichimo et al., 2010; McCarthy et al., 2015b), at 34.5°S MOC variability appears to be

more complicated. At 34.5°S, eastern boundary density variations are the most important at the interannual time scales during 2009-2017, but the western boundary density contributions are still significant, and barotropic changes dominate in some years. Baroclinic (density-driven) and barotropic (bottom pressure-driven) changes at both boundaries are clearly important at seasonal time scales. At time scales shorter than semi-annual, variations at the western boundary meet or exceed those of the eastern boundary, although this may solely be a function of where the mooring locations are relative to the Brazil and Benguela Currents. Planned augmented observations on the continental shelves and upper slopes will aid in the future in evaluating the sensitivity of the estimated MOC by better capturing the near-shore transports, and will improve the overall accuracy of these MOC estimates. The observations presented here demonstrate unequivocally that the dynamical control of the MOC flows at 34.5°S is more broadly spread across the basin than at 26.5°N. This is likely due to the South Atlantic basin's role as a 'mixing pot' for exchange with the Indian and Pacific basins. These measurements also illustrate the essentiality of continuous daily observations to avoid aliasing of highly energetic short period variations, and the strong need to independently observe both the baroclinic (density gradient driven) and barotropic components of the MOC flow at both boundaries.

Acknowledgements:

The authors would like to thank the ship captains and crews who have supported our research cruises. Thanks also to the support/technical teams in Miami, São Paulo, Buenos Aires, Cape Town, and Brest who have helped collect and process the data presented herein. The U.S. PIES observations and the participation of CM, RP, SD, and SG were supported via the NOAA Climate Program Office-Ocean Observing and Monitoring Division (FundRef# 100007298) under the Southwest Atlantic Meridional Overturning Circulation ("SAM") project. SG, MLH, and MK were supported in part under the auspices of the Cooperative Institute for Marine and Atmospheric Studies (CIMAS), a Cooperative Institute of the University of Miami and NOAA, cooperative agreement NA10OAR4320143, and under a grant from the NOAA Climate Variability Program (GC16-212). RP acknowledges additional support from NOAA (Grant NA13OAR4310131) and NASA (Grant NNX14AH60G). CM, RP, SD, SG, MLH, and MK also acknowledge additional support from

the NOAA Atlantic Oceanographic and Meteorological Laboratory. SS and TT acknowledge support from the 11-ANR-56-004 SAMOC research project. SS also received support from the European Union Horizon 2020 research and innovation programme under grant agreement 633211 (AtlantOS). EC and OS acknowledge CNPq for a Research Fellowship (Grant 302018/2014-0) and FAPESP for support through the SAMOC-Br project (Grants 2011/50552-4 and 2017/09659-6). IA, TL, and MvdB acknowledge support from the DST-NRF-SANAP programme and the South African DEA. Additional support for AP, EC, MPC and DV was provided by the Inter-American Institute for Global Change Research grant CRN3070 (US NSF grant GEO-1128040). The CCMP version 2.0 wind product was created by Remote Sensing Systems and is made available on the web at www.remss.com. Helpful comments from the anonymous reviewers on an earlier draft of this manuscript were appreciated. More information about obtaining the data from the South Atlantic MOC Basin-wide Array (SAMBA) can be found at: www.aoml.noaa.gov/phod/SAMOC_international/index.php.

References:

Ansorge I., M. Baringer, E. Campos, S. Dong, R. A. Fine, S. Garzoli , G. Goni, C. Meinen, R. Perez, A. Piola, M. Roberts, S. Speich, J. Sprintall, T. Terre, and M. van den Berg, Basin-wide oceanographic array bridges the South Atlantic, *EOS Transactions*, AGU, 95(6), 53-54, 10.1002/2014EO060001, 2014.

Atlas, R., R. N. Hoffman, J. Ardizzone, S. M. Leidner, J. C. Jusem, D. K. Smith, and D. Gombos, A cross-calibrated, multiplatform ocean surface wind velocity product for meteorological and oceanographic applications, *Bull. Amer. Meteor. Soc.*, 92, 157-174, doi: 10.1175/2010BAMS2946.1, 2011.

Atlas, R., R. N. Hoffman, S. C. Bloom, J. C. Jusem, and J. Ardizzone, A multiyear global surface wind velocity dataset using SSM/I wind observations, *Bull. Amer. Meteor. Soc.*, 77, 5, 869-882, 1996.

Bryden, H. L., B. A. King, and G. D. McCarthy, South Atlantic overturning circulation at 24°S, *J. Mar. Res.*, 69, 39-56, doi:10.1357/002224011798147633, 2011.

Buckley, M. W., and J. Marshall, Observations, inferences, and mechanisms of the Atlantic Meridional Overturning Circulation: A review, *Rev. Geophys.*, 54, 5-63, doi:10.1002/2015RG000493, 2016.

Chidichimo, M. P., T. Kanzow, S. A. Cunningham, W. E. Johns, and J. Marotzke, The contribution of eastern-boundary density variations to the Atlantic Meridional Overturning Circulation at 26.5°N, *Ocean Sci.*, 6, 475-490, 2010.

Cunningham, S. A., T. Kanzow, D. Rayner, M. O. Baringer, W. E. Johns, J. Marotzke, H. R. Longworth, E. M. Grant, J. J.-M. Hirschi, L. M. Beal, C. S. Meinen, and H. L. Bryden, Temporal variability of the Atlantic Meridional Overturning Circulation at 26.5°N, *Science*, 317, 935, doi: 10.1126/science.1141304, 2007.

de Ruijter, W. P. M., A. Biastoch, S. S. Drijfhout, J. R. E. Lutjeharms, R. P. Matano, T. Pichevin, P. J. van Leeuwen, and W. Weijer, Indian-Atlantic interocean exchange: Dynamics, estimation and impact, *J. Geophys. Res.*, 104 (C9), 20885-20910, 1999.

Dijkstra, H. A., Characterization of the multiple equilibria regime in a global ocean model, *Tellus, Ser. A*, 59, 695–705, 2007.

Dong, S., S. L. Garzoli, M. O. Baringer, C. S. Meinen, and G. J. Goni, The Atlantic Meridional Overturning Circulation and its northward heat transport in the South Atlantic, *Geophys. Res. Lett.*, 36, L20606, doi:10.1029/2009GL039356, 2009.

Dong, S., M. O. Baringer , G. J. Goni , C. S. Meinen , and S. L. Garzoli**,** Seasonal variations in the South Atlantic Meridional Overturning Circulation from observations and numerical models, *Geophys. Res. Lett*., 41, 4611-4618, doi:10.1002/2014GL060428, 2014.

Dong, S., G. Goni , and F. Bringas, Temporal variability of the Meridional Overturning Circulation in the South Atlantic between 20°S and 35°S, *Geophys. Res. Lett.*, 42, 7655 - 7662, doi:10.1002/2015GL065603, 2015.

Drijfhout, S. S., S. L. Weber, and E. van der Swaluw, The stability of the MOC as diagnosed from model projections for pre-industrial, present and future climates, *Clim. Dyn.*, 37, 1575-1586, doi:10.1007/s00382-010-0930-z, 2011.

Frajka-Williams, E., C. S. Meinen, W.E. Johns, D.A. Smeed, A. Duchez, A.J. Lawrence, D.A. Cuthbertson, G.D. McCarthy, H.L. Bryden, M.O. Baringer, B.I. Moat, and D. Rayner, Compensation between meridional flow components of the AMOC at 26°N, *Ocean Sci.*, 12, 481-493, doi:10.5194/os-12-481-2016, 2016.

Garzoli, S. L., and A. L. Gordon, Origins and variability of the Benguela Current, *J. Geophys. Res.*, 101 (C1), 897-906, 1996.

Garzoli, S. L., and M.O. Baringer, Meridional heat transport determined with expendable bathythermographs, Part II: South Atlantic transport, *Deep-Sea Res. I*, 54(8), 1402-1420, 2007.

Garzoli, S. L and R. Matano, The South Atlantic and the Atlantic Meridional Overturning Circulation, *Deep-Sea Res. II*, 58, 1837-1847, doi:10.1016/j.dsr2.2010.10.063, 2011.

Garzoli, S., M. O. Baringer, S. Dong, R. Perez, and Q. Yao, South Atlantic meridional fluxes, *Deep-Sea Res. I,* 71, 21-32, doi:10.1016/j.dsr.2012.09.003, 2013.

Goni, G. J, F. Bringas, and P. N. DiNezio, Observed low frequency variability of the Brazil Current front, *J. Geophys. Res.*, 116, C10037, doi: 10.1029/2011JC007198, 2011.

Hall, C., and J. R. E. Lutjeharms, Cyclonic eddies identified in the Cape Basin of the South Atlantic Ocean, *J. Mar. Sys.*, 85, 1-10, doi: 10.1016/j.jmarsys.2010.10.003, 2011.

Hermes, J. C., C. J. C. Reason, and J. R. E. Lutjeharms, Modeling the variability of the Greater Agulhas Current System, *J. Clim.*, 20, 3131-3146, doi: 10.1175/JCLI4154.1, 2007.

Hoffman, R. N., M. Leidner, J. M. Henderson, R. Atlas, J. V. Ardizzone, and S. C. Bloom, A two-dimensional variational analysis method for NSCAT ambiguity removal: methodology, sensitivity, and tuning, *J. Atmos. Oceanic Tech.*, 20, 585-605, 2013.

Huisman, S. E., M. Den Toom, H. A. Dijkstra, An indicator of the multiple equilibria regime of the Atlantic Meridional Overturning Circulation, *J. Phys. Oceanogr.*, 40, 551-567, 2010.

Kanzow, T., S. A. Cunningham, D. Rayner, J. J-M. Hirshi, W. E. Johns, M. O. Baringer, H. L. Bryden, L. M. Beal, C. S. Meinen, and J. Marotzke, Observed flow compensation associated with the meridional overturning at 26.5°N in the Atlantic, *Science*, 317, 938-940, doi: 10.1126/science.1141293, 2007.

Kanzow, T., S. A. Cunningham, W. E. Johns, J. J-M. Hirschi, J. Marotzke, M. O. Baringer, C. S. Meinen, M. P. Chidichimo, C. Atkinson, L. M. Beal, H. L. Bryden, and J. Collins, Seasonal variability of the Atlantic Meridional Overturning Circulation at 26.5°N, *J. Clim.*, 23(21), 5678-5698, 2010.

Kersalé, M., T. Lamont, S. Speich, T. Terre, R. Laxenaire, M. J. Roberts, M. A. van den Berg, and I. Ansorge, Moored observations of mesoscale features in the Cape Basin: Characteristics and local impacts on water mass distributions, *Ocean Sci. Discuss.*, doi: 10.5194/os-2017-85, (submitted), 2018.

Latif, M., N. Keenlyside, and J. Bader, Tropical sea surface temperature, wind shear, and hurricane development, *Geophys. Res. Lett.*, 34, L01710, doi:10.1029/2006GL027969, 2007.

Lopez, H., S. Dong, S.-K. Lee, and G. Goni, Decadal modulations of interhemispheric global atmospheric circulations and monsoons by the South Atlantic Meridional Overturning Circulation, *J. Clim.*, 29(3), 1831-1851, doi:10.1175/JCLI-D-15-0491.1, 2016.

Lumpkin, R., and K. Speer, Global ocean meridional overturning, *J. Phys. Oceanogr.*, 37, 2550-2562, doi:10.1175/JPO3130.1, 2007.

Majumder, S., C. Schmid, and G. Halliwell, An observations and model-based analysis of meridional transport in the South Atlantic, *J. Geophys. Res. Oceans*, 121, doi:10.1002/2016JC011693, 2016.

Masumoto, Y., H. Sasaki, T. Kagimoto, N. Komori, A. Ishida, Y. Sasai, T. Miyama, T. Motoi, H. Mitsudera, K. Takahashi, H. Sakuma, and T. Yamagata, A fifty-year eddy resolving simulation of the world ocean – Preliminary outcomes of OFES (OGCM for the Earth simulator), *J. Earth Simulator*, 1, 35-56, 2004.

McCarthy, G., E. McDonagh, and B. King, Decadal variability of thermocline and intermediate waters at 24°S in the South Atlantic, *J. Phys. Oceanogr.*, 41, 157-165, 2011.

McCarthy, G. D., I. D. Haigh, J. J. Hirschi, J. P. Grist, D. A. Smeed, Ocean impact on decadal Atlantic climate variability revealed by sea-level observations, *Nature*, 521, 508–510, doi:10.1038/nature14491, 2015a.

McCarthy, G. D., D. A. Smeed, W. E. Johns, E. Frajka-Williams, B. I. Moat, D. Rayner, M. O. Baringer, C. S. Meinen, J. Collins, and H. L. Bryden, Measuring the Atlantic Meridional Overturning Circulation at 26°N, *Prog. Oceanogr.*, 130, 91-111, 2015b.

Meinen, C. S. and Watts, D. R., Vertical structure and transport on a transect across the North Atlantic Current near 42°N: Time series and mean, *J. Geophys. Res.*, 105, 21869–21892, 2000.

Meinen, C. S., A. R. Piola, R. C. Perez, and S. L. Garzoli, Deep Western Boundary Current transport variability in the South Atlantic: Preliminary results from a pilot array at 34.5°S, *Ocean Sci.*, 8, 1041-1054, doi:10.5194/os-8-1041-2012, 2012.

Meinen, C, S ., S. Speich, R. C. Perez , S. Dong , A. R. Piola, S. L. Garzoli , M. O. Baringer, S. Gladyshev, and E. J. D. Campos, Temporal variability of the Meridional Overturning Circulation at 34.5°S: Results from two pilot boundary arrays in the South Atlantic, *J. Geophys. Res.-Oceans*, 118, 6461-6478, doi:10.1002/2013JC009228, 2013.

Meinen, C. S., S. L. Garzoli, R. C. Perez, E. Campos, A. R. Piola, M.-P. Chidichimo, S. Dong, and O. T. Sato, Characteristics and causes of Deep Western Boundary Current

transport variability at 34.5°S during 2009-2014, *Ocean Sci.*, 175-194, doi:10.5194/os-13-175-2017, 2017.

Olson, D. B., G. P. Podesta, R. H. Evans, and O. B. Brown, Temporal variations in the separation of the Brazil and Malvinas Currents, *Deep-Sea Res.*, 35 (12), 1971-1990, 1988.

Perez, R. C., S. L. Garzoli, C. S. Meinen, and R. P. Matano, Geostrophic velocity measurement techniques for the Meridional Overturning Circulation and meridional heat transport in the South Atlantic, *J. Atmos. Oceanic Technol.*, 28, 1504–1521, doi:10.1175/JTECH-D-11-00058.1, 2011.

Rayner, D., J. J.-M. Hirschi, T. Kanzow, W. E. Johns, P. G. Wright, E. Frajka-Williams, H. L. Bryden, C. S. Meinen, M. O. Baringer, J. Marotzke, L. M. Beal, and S. A. Cunningham, Monitoring the Atlantic Meridional Overturning Circulation, *Deep-Sea Res. II*, 58, 1744-1753, doi: 10.1016/j.dsr2.2010.10.056, 2011.

Rintoul, S. R., South Atlantic interbasin exchange, *J. Geophys. Res.*, 96, 2675-2692, 1991.

Sasaki, H., M. Nonaka, Y. Sasai, H. Uehara, and H. Sakuma, An eddy-resolving hindcast simulation of the quasiglobal ocean from 1950 to 2003 on the Earth simulator, in *High Resolution Numerical Modelling of the Atmosphere and Ocean*, edited by K. Hamilton and W. Ohfuchi, pp. 157–185, Springer, New York, 2008.

Sloyan, B. M., and S. R. Rintoul, The southern limb of the global deep overturning circulation, *J. Phys. Oceanogr.*, 31 (1), 143-173, 2001.

Smeed, D. A., S. A. Josey, C. Beaulieu, W. E. Johns, B. I. Moat, E. Frajka-Williams, D. Rayner, C. S. Meinen, M. O. Baringer, H. L. Bryden, and G. D. McCarthy, The North Atlantic Ocean is in a state of reduced overturning, *Geophys. Res. Lett.*, (in press), doi: 10.1002/2017GL076350, 2018.

Smith, W. H. F., and D. T. Sandwell, Global sea floor topography from satellite altimetry and ship depth soundings, *Science*, 277 (5334), l956-1962, 1997.

Stouffer, R. J., J. Yin, and J. M. Gregory, Investigating the causes of the response of the thermohaline circulation to past and future climate changes, *J. Clim.*, 19(8), 1365–1387, 2006.

Vellinga, M., and R. A. Wood, Global climatic impacts of a collapse of the Atlantic thermohaline circulation, *Clim. Change*, 54(3), 251–267, 2002.

Wentz, F. J., J. Scott, R. Hoffman, M. Leidner, R. Atlas, and J. Ardizzone, Remote Sensing Systems Cross-Calibrated Multi-Platform (CCMP) 6-hourly ocean vector wind analysis product on 0.25 deg grid, Version 2.0, Remote Sensing Systems, Santa Rosa, CA, Available online at www.remss.com/measurements/ccmp, 2015.

Table 1: Annual average MOC transport anomalies relative to the record-length mean: Total MOC (bold, top row), Ekman contribution, relative velocity (density gradient) contribution, and reference velocity (bottom pressure gradient) contribution are shown. Positive values denote anomalous northward flow. For the relative and reference velocity contributions, the results are further broken down into the contributions due to the western and eastern boundary density (relative) or pressure (reference) variations. Annual averages are calculated by calendar year between January 1 and December 31. Years with fewer than nine months of daily observations available for averaging are denoted by gray italics (2013 and 2017). Final column shows the statistical standard error of the mean (SEM) for each contribution (average of the values from each of the five full years), based on calculated integral time scales of 9, 7, 15, and 10 days for the total, Ekman, relative, and reference components, respectively.

	2009	2010	*2013*	2014	2015	2016	*2017*	SEM
Total MOC	**4.6 Sv**	**-1.8 Sv**	***-3.4 Sv***	**-3.8 Sv**	**3.2 Sv**	**0.3 Sv**	***-1.9 Sv***	**1.7 Sv**
Ekman contribution	0.7 Sv	-0.6 Sv	*-1.2 Sv*	-0.0 Sv	-0.1 Sv	0.5 Sv	*-2.3 Sv*	0.9 Sv
Relative contribution	4.2 Sv	0.3 Sv	*-3.5 Sv*	-4.2 Sv	0.9 Sv	-0.1 Sv	*-2.5 Sv*	1.5 Sv
Reference contribution	-0.3 Sv	-1.3 Sv	*1.0 Sv*	0.4 Sv	2.1 Sv	-0.4 Sv	*2.6 Sv*	1.0 Sv
West density contribution	1.8 Sv	-1.3 Sv	*-0.4 Sv*	-1.3 Sv	1.8 Sv	-1.4 Sv	*-2.3 Sv*	1.1 Sv
East density contribution	2.5 Sv	1.6 Sv	*-3.2 Sv*	-2.9 Sv	-0.9 Sv	1.3 Sv	*-0.2 Sv*	1.2 Sv
West pressure contribution	0.4 Sv	-0.3 Sv	*0.4 Sv*	0.0 Sv	0.9 Sv	-0.3 Sv	*0.2 Sv*	0.9 Sv
East pressure contribution	-0.8 Sv	-1.1 Sv	*0.5 Sv*	0.2 Sv	1.0 Sv	-0.1 Sv	*2.2 Sv*	0.8 Sv

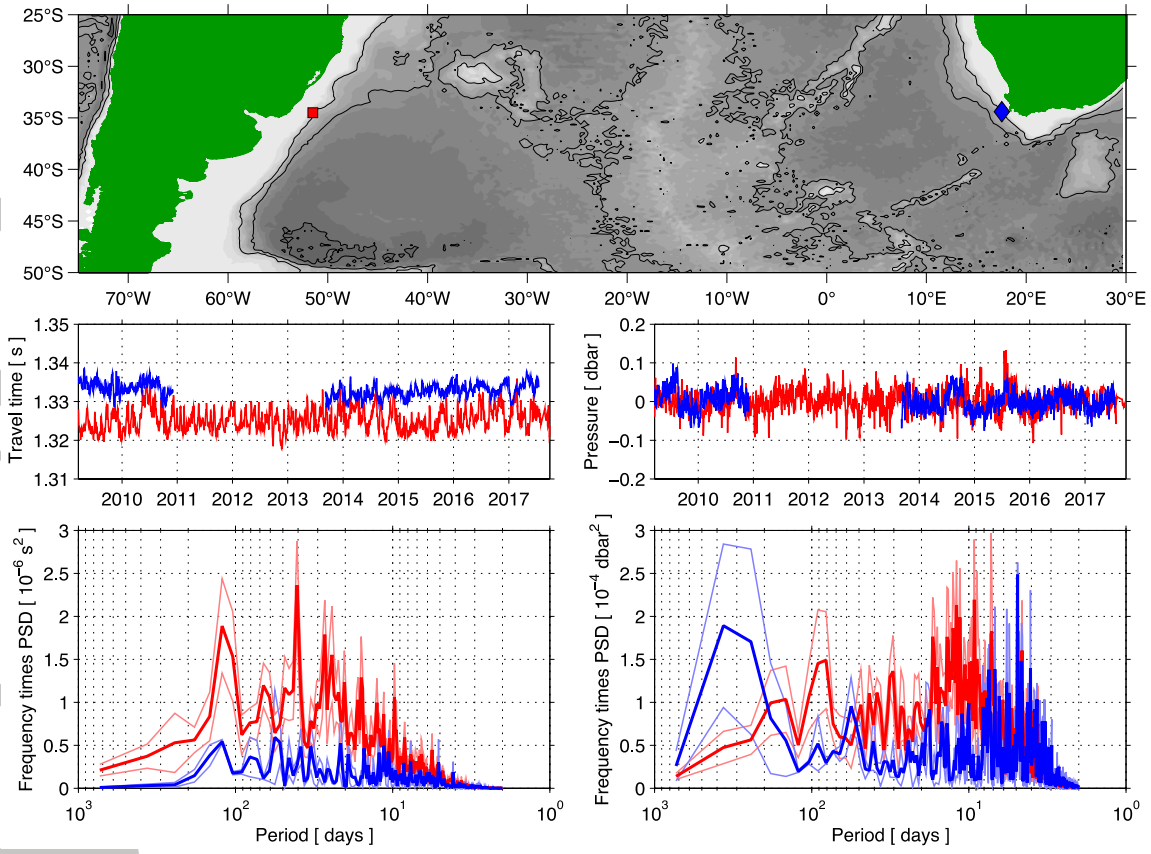

Figure 1: (a) Map showing the two moored instrument locations, Site A in the west (red) and Site Z in the east (blue), both located close to the 1350 dbar isobath; (b) daily measured round-trip acoustic travel time records, calibrated to an effective pressure level of 1000 dbar, at the western (red) and eastern (blue) sites; (c) daily measured bottom pressure records at the western (red) and eastern (blue) sites; (d) variance preserving spectra of the travel time records at the western (red) and eastern (blue) sites; (e) variance preserving spectra of the bottom pressure records at the western (red) and eastern (blue) sites. Note that the spectra for the Site Z data were computed using the continuous ~4-year records available from 2013-2017. Spectra were determined via the Welch's averaged periodogram method using a 2-year window allowing 1-year of overlap; thin lines in spectra indicate 67% confidence limits. Topography in the top panel (gray shading with 500 m intervals; every 2000 m contour shown as black contour) is from Smith and Sandwell (1997).

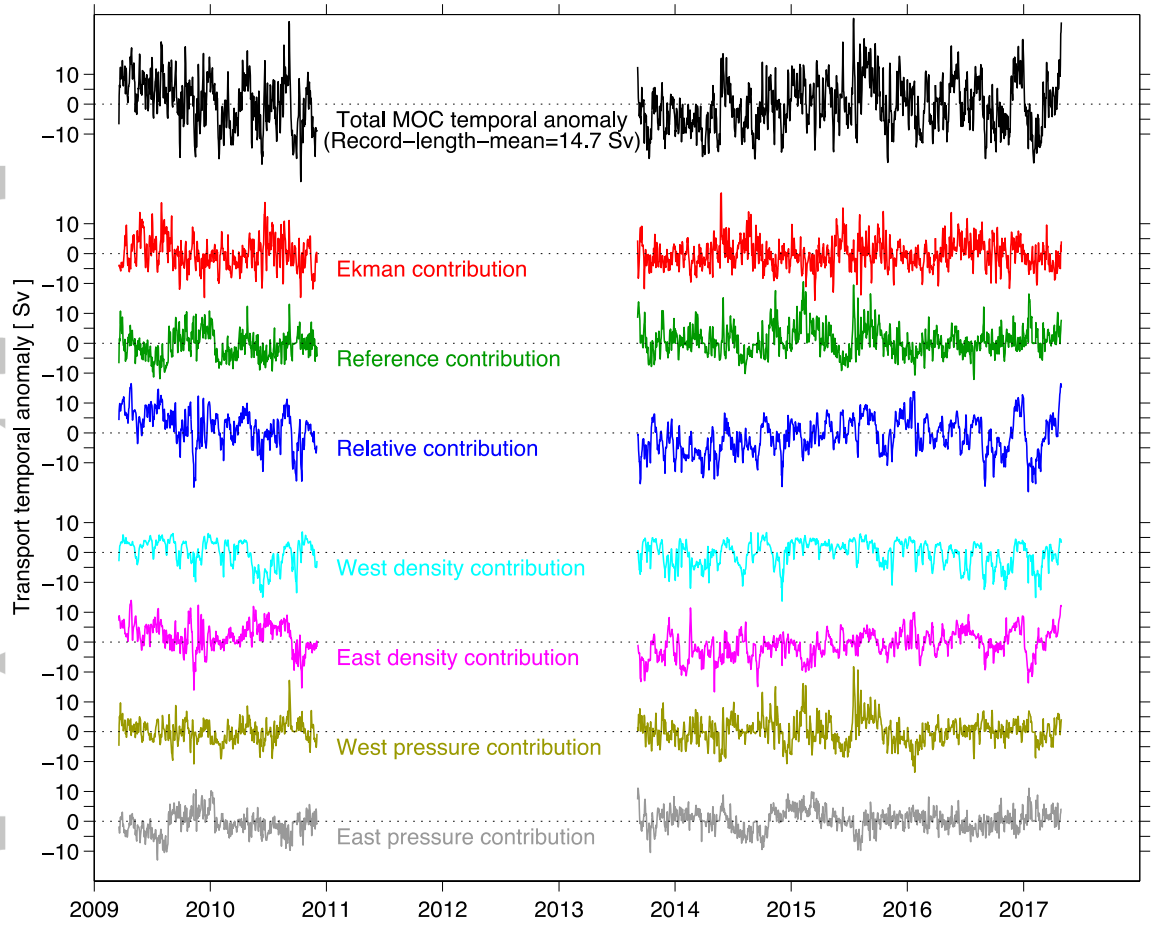

Figure 2: Time series (temporal anomaly relative to the record-length mean) of the basin-wide MOC volume transport across 34.5°S calculated as described in the text. The total (net) transport anomaly is shown in black. The record-length mean total MOC value that has been removed to create the anomaly is noted on the figure. Also shown are the contributions of Ekman, geostrophic reference flow, and geostrophic relative flow components; the geostrophic relative and reference flow components are further broken down into the contributions from variations in the western and eastern density or pressure contributions, respectively. For all components, the 'contribution' is estimated as the difference between the total MOC (black line) and the MOC calculated while holding the term in question constant (i.e. the reference contribution is the difference between the total MOC and the MOC that was calculated holding the bottom pressure values on both sides of the basin constant).

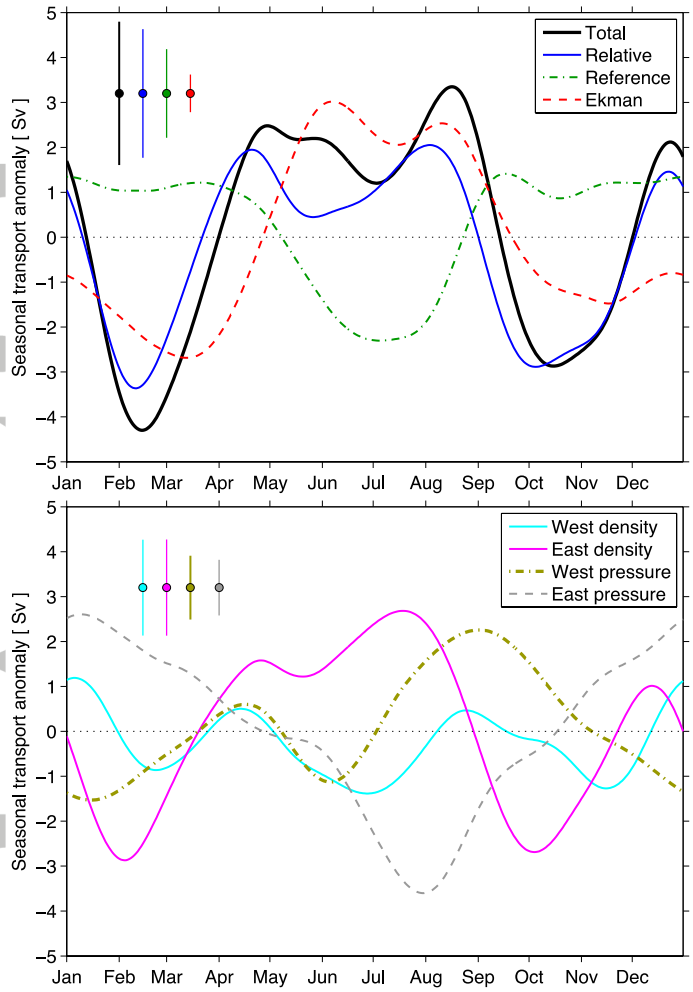

Figure 3: (a) Seasonal anomaly of the MOC volume transport time series. The seasonal anomaly of the total, geostrophic relative, geostrophic reference, and Ekman transports are shown. (b) Seasonal anomalies resulting from variations on either end of the basin for the relative component (density) and the reference component (pressure). All anomalies in both panels are determined using the continuous daily 2009-2010 and 2013-2017 data, with each daily climatology smoothed with a second-order Butterworth low-pass filter using a 90-day cutoff period passed both forward and backward to avoid phase shifting. A three-repeating-year climatology is used for the filtering, and only the central year is kept to eliminate edge effects/transients in the smoothed climatology. Error bars indicated in the upper left of each panel represent plus/minus one standard error, with colors matching the corresponding time series. The standard error is calculated as the standard deviation of the difference between the 90-day low-pass filtered daily data and the corresponding daily climatology, divided by the square-root of the number of years of data available.